

A Unified Framework for Iris Anti-Spoofing: Introducing IrisGeneral Dataset and Masked-MoE Method

Hang Zou^{1*}, Chenxi Du^{2,3*}, Ajian Liu⁴, Yuan Zhang¹, Jing Liu⁵, Mingchuan Yang¹, Jun Wan⁴, Hui Zhang^{5†}

¹China Telecom Research Institute (CTRI), China;

²SIAT, Chinese Academy of Sciences, China; ³Southern University of Science and Technology, China;

⁴MAIS, CASIA, China; ⁵Tianjin University of Science & Technology, China.

¹zouh3@chinatelecom.cn; ²cxdu025@163.com; ⁵zhanghui2022@tust.edu.cn.

Abstract

Iris recognition is widely used in high-security scenarios due to its stability and distinctiveness. However, the acquisition of iris images typically requires near-infrared illumination and near-infrared band filters, leading to significant and consistent differences in imaging across devices. This underscores the importance of developing cross-domain capabilities in iris anti-spoofing methods. Despite this need, there is no dataset available that comprehensively evaluates the generalization ability of the iris anti-spoofing task. To address this gap, we propose the IrisGeneral dataset, which includes 10 subsets, belonging to 7 databases, published by 4 institutions, collected with 6 types of devices. IrisGeneral is designed with three protocols, aimed at evaluating average performance, cross-racial generalization, and cross-device generalization of iris anti-spoofing models. To tackle the challenge of integrating multiple sub-datasets in IrisGeneral, we employ multiple parameter sets to learn from the various subsets. Specifically, we utilize the Mixture of Experts (MoE) to fit complex data distributions using multiple sub-neural networks. To further enhance the generalization capabilities, we introduce a novel method Masked-MoE (MMoE). It randomly masks a portion of tokens for some experts and requires their outputs to be similar to the unmasked experts, which improves the generalization ability and effectively mitigates the overfitting issue produced by MoE. We selected ResNet50, ViT-B/16, CLIP, and FLIP as representative models and benchmarked them on the IrisGeneral dataset. Experimental results demonstrate that our proposed MMoE with CLIP achieves the best performance on IrisGeneral.

Introduction

The iris is inside the eye and has large differences between each human, which is stable and distinguishable (Agarwal and Jalal 2021), making it widely used in high-security scenarios. Thus it is necessary to ensure the security of the iris recognition system because it always relates to the property and critical areas (Nigam, Vatsa, and Singh 2015; Peralta 2017; Gent 2023). Iris recognition systems are similar to other kinds of biometric detection systems that are weak to spoofing such as paper prints, screens, contact lenses, and plastic eyes (Yadav, Chen, and Ross 2019, 2020). Among

*These authors contributed equally.

†Corresponding author.

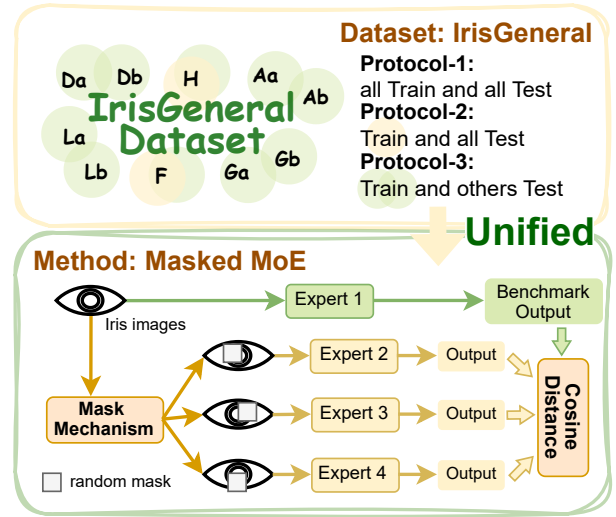


Figure 1: The unified framework for iris anti-spoofing is shown in this Figure. Including the IrisGeneral dataset and the Masked-MoE method.

those, contact lenses are complicated to detect because they are worn on real eyeballs and can deceive liveness detection systems (Bowyer and Doyle 2014; Galbally et al. 2012). They are transparent with some textures, so the iris texture and the contact lens texture are intertwined, making them difficult to classify.

Some previous work has been performed to combat contact lens attacks, such as 2D Gabor wavelet-based iris recognition (Daugman 2009), and 4DCycle-GAN (Zou et al. 2018). They trained on specific datasets and showed good results, but may not be able to cope with the problem once the acquisition equipment is changed. The near-infrared fill light bands, camera filters, collection distances, and ambient light, make a lot of impact on iris acquisition which requires near-infrared presentation (Xiao et al. 2013). The image-imaging differences between each iris acquisition device are obvious and fixed. This means that the cross-domain ability of the iris anti-spoofing methods is necessary, thus the security could be maintained more effectively. However, there are no suitable iris datasets to train and evaluate iris anti-spoofing mod-

DataBase	Dataset	Devices.	Nickname	Num of Train (Real / Fake)	Num of Test (Real / Fake)	Num of Total
CASIAH100	CASIAH100	H100	H	4806 / 592	1198 / 148	6744
Clarkson 2013 for LivDet-Iris 2013	Clarkson2013Dalsa	DALSA	Da	270 / 400	246 / 440	1356
Clarkson 2015 for LivDet-Iris 2015	Clarkson2015Dalsa	DALSA	Db	700 / 873	378 / 558	2509
	Clarkson2015LG2200	LG2200	La	450 / 540	378 / 576	1944
Clarkson 2017 dataset for LivDet-Iris 2017	Clarkson2017LG2200	LG2200	Lb	2469 / 1122	1485 / 765	5841
IFVE	IFVEAI1000	AI1000	F	20000 / 20000	5000 / 5000	50000
Notre Dame 2013 for LivDet-Iris 2013	ND2013LG4000	LG 4000	Ga	2000 / 1000	800 / 400	4200
	ND2013AD100	AD 100 sensor	Aa	400 / 200	200 / 100	900
Notre Dame 2017 for LivDet-Iris 2017	ND2017LG4000	LG 4000	Gb	600 / 600	900 / 900	3000
	ND2017-CDAD100	AD 100 sensor	Ab	0	900 / 900	1800

Table 1: This Table shows the scale of the sub-datasets employed in the IrisGeneral dataset, including the numbers of real and fake samples in both training and testing sets. The first letters of the nicknames denote the collection devices while the second letters denote the order to distinguish.

els’ generalization on cross-domain adaptation (Yadav and Ross 2024). To address that, we proposed this IrisGeneral dataset, which includes 10 subsets, belonging to 7 databases, published by 4 institutions, and collected with 6 types of devices. It is designed with three protocols, aimed at evaluating average performance, cross-racial generalization, and cross-device generalization of iris anti-spoofing models. Section IrisGeneral Dataset provides the details of this dataset.

The IrisGeneral brings the challenge of integrating multiple sub-datasets with different racial and devices. To tackle it, we employ multiple parameter sets to learn from the various subsets by using the Mixture of Experts (MoE) (Jacobs et al. 1991) to fit complex data distributions with multiple sub-neural networks. However, some previous works have found that sparse MoE would bring overfitting problems into models (Shazeer et al. 2017; Chen et al. 2023; Elbayad, Sun, and Bhosale 2022; Lepikhin et al. 2020). At the same time, overfitting is also the main challenge of the iris anti-spoofing task, which is caused by its high structural homogeneity, leading to the differences between live iris and fake iris mainly in their fine textures. Thus, alleviating the overfitting and improving the generalization of the model is necessary. To address that, we introduce a novel Masked-MoE (MMoE) method to enhance the generalization capabilities. It has two contributions: Mask Mechanism to alleviate overfitting, and Cosine Distance Loss to further improve the model’s generalization. Specifically, the Mask Mechanism masks parts of the input tokens for several experts and allows one expert to see all tokens with complete information. Then the Cosine Distance Loss requests the output of masked experts to be similar to the unmasked experts as shown in Figure 1. It is inspired by MAE (He et al. 2022), and we refer to this masking method to improve the generalization to deal with the inherent overfitting problem of MoE. Section Proposed Method provides the details of our MMoE method. To evaluate our contributions, we selected ResNet50, ViT-B/16, CLIP, and FLIP as representative models and benchmarked them on the

IrisGeneral dataset. Experimental results show that our proposed MMoE with CLIP has strong generalization abilities and achieves the best performance on both three protocols, section Experiment provides more details.

The main contributions in this paper are shown as follows:

- **We proposed a unified framework for Iris Anti-Spoofing**, including IrisGeneral dataset and Masked-MoE method.
- **Dataset:** The IrisGeneral dataset is proposed with three protocols that could respectively evaluate the average, cross-racial, and cross-device performance of the iris-antispoofing task.
- **Method:** The Masked-MoE (MMoE) method is proposed with the Mask Mechanism and the Cosine Distance Loss, which efficiently alleviates the problem of MoE method overfitting and improves the models’ generalization.

Related Work

Iris Anti-Spoofing

Detecting contact lenses is a complicated task of iris recognition system. Many previous research focuses on this, including traditional and deep-learning-based methods (Yadav and Ross 2024; Kumar, Lamba, and Jangra 2020). Wei et al. (Wei et al. 2008) proposed a method to detect the sharpness of the edge of the iris. He et al. (He, An, and Shi 2007) conducted classification through a feature vector and support vector machine based on GLCM. J. Komulainen et al. (Komulainen, Hadid, and Pietikäinen 2014) studied the generalized cases of software-based device-independent detection of contact lens. Many studies deal the iris anti-spoofing by neural networks such as CNN (LeCun et al. 1998) or generative network-based methods (Goodfellow et al. 2014; Kingma and Welling 2013), and etc. For example, (Yadav et al. 2014a), and (Tinsley, Flynn, and Czajka 2024; Boyd et al. 2021).

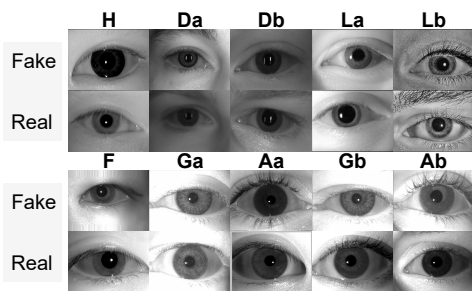


Figure 2: Some image samples of the IrisGeneral dataset. Include 10 subsets with Real and Fake iris images.

Cross-domain Adaption

Cross-domain adaption measures the models’ ability to transfer the knowledge learned in the source domain to the target domain. Two main directions to improve are as follows. One is introducing an adversarial discriminator (Tzeng et al. 2017) to bring the source domain and the target domain closer. The other direction is extracting the features of source and target domain with one neural network (Ren et al. 2020). A loss function is designed to measure the distance between the two domains. There also some previous works which proposed effective methods to improve the adaption, for example, DAN (Long et al. 2015), MMD (Yadav et al. 2014b), and JAN (Long et al. 2017).

IrisGeneral Dataset

Subsets Detail

There are 10 subsets, belonging to 7 databases, published by 4 institutions, collected with 6 types of devices in the Iris-General Dataset. Table 1 lists the information of each subset. Figure 2 provides some real and fake iris image samples of each subset.

CASIAH100 (Sun et al. 2014) with 6744 samples in total, collected by H100, belonging to database CASIAH100, contains 5398 samples in its training set and 1346 samples in its testing set. We call this dataset H in short.

Clarkson2013Dalsa (Yambay et al. 2017) with 1356 samples in total, collected by DALSA, belonging to database Clarkson 2013 for LivDet-Iris 2013, contains 670 samples in its training set and 686 samples in its testing set. We call this dataset Da in short.

Clarkson2015Dalsa (Yambay et al. 2017) with 2509 samples in total, collected by DALSA, belonging to database Clarkson 2015 for LivDet-Iris 2015, contains 1573 samples in its training set and 936 samples in its testing set. We call this dataset Db in short.

Clarkson2015LG2200 (Yambay et al. 2017) with 1944 samples in total, collected by LG2200, belonging to database Clarkson 2015 for LivDet-Iris 2015, contains 990 samples in its training set and 954 samples in its testing set. We call this dataset La in short.

Clarkson2017LG2200 (Yambay et al. 2017) with 5841 samples in total, collected by LG2200, belonging to the

Dataset	P1	P2	P3.1	P3.2	P3.3	P3.4	P3.5	P3.6
H	✓/✓	✓/✓	-/✓	✓/-	✓/-	✓/-	✓/-	✓/-
Da	✓/✓	-/✓	✓/-	-/✓	✓/-	✓/-	✓/-	✓/-
Db	✓/✓	-/✓	✓/-	-/✓	✓/-	✓/-	✓/-	✓/-
La	✓/✓	-/✓	✓/-	✓/-	-/✓	✓/-	✓/-	✓/-
Lb	✓/✓	-/✓	✓/-	✓/-	-/✓	✓/-	✓/-	✓/-
F	✓/✓	✓/✓	✓/-	✓/-	✓/-	-/✓	✓/-	✓/-
Ga	✓/✓	-/✓	✓/-	✓/-	✓/-	✓/-	-/✓	✓/-
Aa	✓/✓	-/✓	✓/-	✓/-	✓/-	✓/-	✓/-	-/✓
Gb	✓/✓	-/✓	✓/-	✓/-	✓/-	✓/-	-/✓	✓/-
Ab	✓/✓	-/✓	✓/-	✓/-	✓/-	✓/-	✓/-	-/✓

Table 2: This table shows the Train / Test usage of each dataset of each protocol. In Protocol-1, all datasets’ training and testing sets are involved. In Protocol-2, training sets are H and F, and testing sets involve all the 10 subsets. In Protocol-3, for each sub-protocol, we choose one device to test, and others to train.

database Clarkson 2017 dataset for LivDet-Iris 2017, contains 3591 samples in its training set and 2250 samples in its testing set. We call this dataset Lb in short.

IFVEAI1000 (Zhang et al. 2021) with 50000 samples in total, collected by AI1000, belonging to database IFVE, contains 40000 samples in its training set and 10000 samples in its testing set. And we call this dataset F in short.

ND2013LG4000 (Doyle and Bowyer 2014) with 4200 samples in total, collected by LG4000, belonging to database Notre Dame 2013 for LivDet-Iris 2013, contains 3000 samples in its training set and 1200 samples in its testing set. We call this dataset Ga in short.

ND2013AD100 (Doyle and Bowyer 2014) with 900 samples in total, collected by AD100sensor, belonging to database Notre Dame 2013 for LivDet-Iris 2013, contains 600 samples in its training set and 300 samples in its testing set. We call this dataset Aa in short.

ND2017LG4000 (Yambay et al. 2017) with 3000 samples in total, collected by LG4000, belonging to database Notre Dame 2017 for LivDet-Iris 2017, contains 1200 samples in its training set and 1800 samples in its testing set. We call this dataset Gb in short.

ND2017-CDAD100 (Yambay et al. 2017) with 1800 samples in total, collected by AD100sensor, belonging to database Notre Dame 2017 for LivDet-Iris 2017, contains 0 samples in its training set and 1800 samples in its testing set. We call this dataset Ab in short.

Protocols of IrisGeneral

Three protocols are defined in the IrisGeneral dataset to evaluate the three kinds of generalization performance of the models. Table 2 shows the Train / Test usage of each dataset.

Protocol-1 evaluates the model’s average performance in iris anti-spoofing, including the training and testing sets of all datasets.

Protocol-2 evaluates the model’s generalization performance of cross-racials. The training sets include H and F, and testing sets include all subsets, because the iris samples

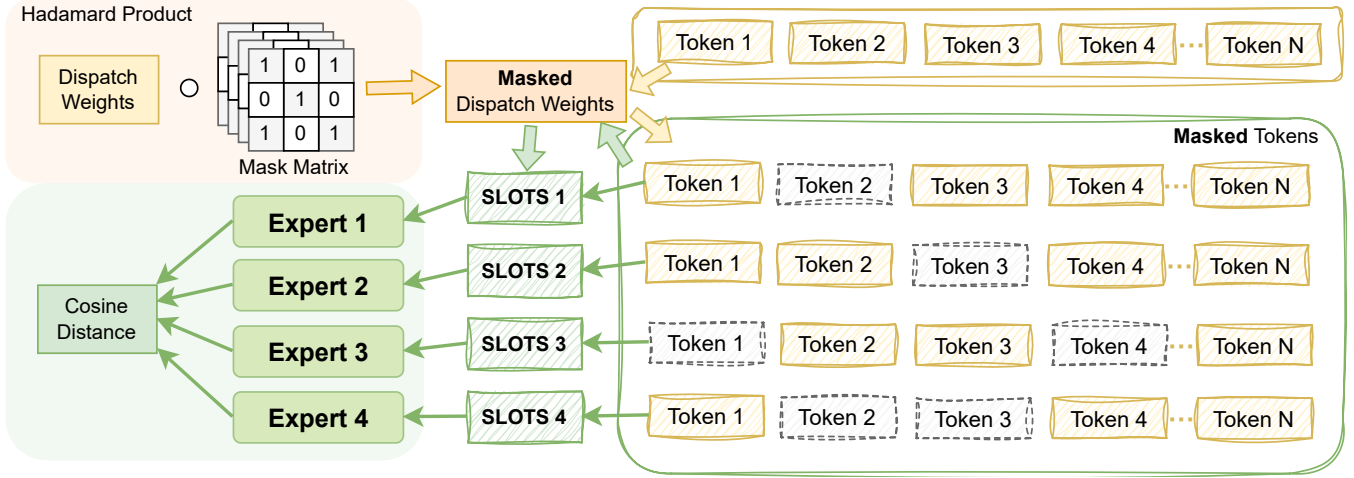


Figure 3: The Masked Mechanism and Cosine Distance Loss of MMoE. After masking the Dispatch Weights with Mask Matrix, the input tokens calculate with it to mask a part of the information, and output the slots. The slots would be input into the expert, then the cosine distance loss calculates the similarity between the output of each expert.

in H and F are totally collected from Asians, while iris samples in other subsets are from multiple races.

Protocol-3 evaluates the model’s generalization performance of cross-devices, with six sub-protocols. The datasets are divided into six parts based on the devices used for collection. In each sub-protocol, five parts are used to train, and the remaining one is used to test.

Proposed Method

In this work, We proposed the Masked-MoE (MMoE) method with two main contributions: Mask Mechanism and Cosine Distance Loss. Figure 3 demonstrates the critical part of the framework, and Algorithm 1 provides the working process, including the details of masking dispatch weights and the measure of cosine distances between experts. The MMoE is based on SoftMoE (Puigcerver et al. 2023), and could easily added to the image encoder of CLIP (Radford et al. 2021) as shown in the Figure 4.

Mask Mechanism of MMoE

The overfitting problem of MoE methods inherits exists and is hard to solve (Aceña et al. 2022; Chang et al. 2013; Allingham et al. 2021; Xie et al. 2023). Inspired by MAE (He et al. 2022), which improves the generalization of auto-encoder architecture by masking patches of samples, we refer to this masking method to improve the generalization to deal with the overfitting of MoE. We proposed a novel approach Mask Mechanism, which is different from the sample-wise masking manner of MAE, it is a feature-wise Mask Mechanism that masks parts of the latent features of images by tokens. To achieve that, we generate a random Mask Matrix with fixed mask rates, then use it to mask the Dispatch Weights by Hadamard product. Then the input tokens are weighted by Masked Dispatch Weights, and thus parts of them are masked as shown in Figure 3.

We first introduce the Dispatch Weights shown in Figure 3. Equation 1 is the definition of Dispatch Weights \mathbf{D} and the weighting process of MMoE’s input.

$$\mathbf{D}_{ij} = \frac{\exp((\mathbf{X}\Phi)_{ij})}{\sum_{i'=1}^n \exp((\mathbf{X}\Phi)_{i'j})}, \quad \tilde{\mathbf{X}} = \mathbf{D}^\top \mathbf{X} \quad (1)$$

$\mathbf{X} \in \mathbb{R}^{n \times d}$ is the input tokens of MMoE, n denotes the number of tokens and d denotes their feature dimension. In MMoE with e experts, each expert deals with s slots where each slot has a corresponding vector of parameters with d -dimension. $\Phi \in \mathbb{R}^{d \times (e \cdot s)}$ is a randomly initialized vector to weight the input tokens. $\mathbf{D} \in \mathbb{R}^{n \times (e \cdot s)}$ is the dispatch weights, which is the result of applying a softmax on the columns of $\mathbf{X}\Phi$. \mathbf{D}_{ij} denotes the element in dispatch weights \mathbf{D} located in the i^{th} column and j^{th} row. $\tilde{\mathbf{X}} \in \mathbb{R}^{(e \cdot s) \times d}$ is the input of Experts, a set of slots. It is obtained by weighting \mathbf{X} with the dispatch weights \mathbf{D} . The scale of our proposed Mask Matrix is the same scale as the one of Dispatch Weights \mathbf{D} , $\mathbf{M} \in \mathbb{R}^{n \times (e \cdot s)}$, which consists only of 0 and 1. The mask rate denotes the proportion of 0 in Mask Matrix. In practice, we employ 4 experts in each block of the backbone of CLIP’s image encoder. Only one expert could get the complete information of all slots, while others could only get the masked slots. And then our Masked Dispatch Weights \mathbf{D}' is the Hadamard product of Dispatch Weights \mathbf{D} and Mask Matrix \mathbf{M} , as shown in Equation 2.

$$\mathbf{D}'_{ij} = \mathbf{D}_{ij} * \mathbf{M}_{ij}, \quad \tilde{\mathbf{X}} = \mathbf{D}'^\top \mathbf{X} \quad (2)$$

\mathbf{D}'_{ij} and \mathbf{M}_{ij} denotes the element in masked dispatch weights \mathbf{D}' and Mask Matrix \mathbf{M} located in the i^{th} column and j^{th} row. \mathbf{X} is then weighted by \mathbf{D}' and we get $\tilde{\mathbf{X}}$, the input of Experts.

Cosine Distance Loss between Experts

The efficiency of MoE methods is mainly thanks to the sparse characteristically, which means that each expert could

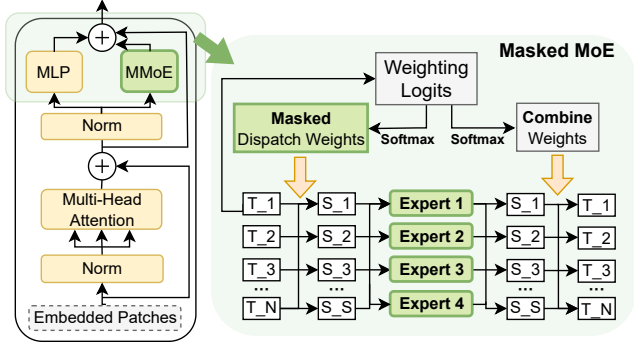


Figure 4: This figure shows the combination framework of MMoE with CLIP. The MMoE block is parallel with the MLP block in the image encoder of the CLIP.

learn different knowledge (Cai et al. 2024). So if we could find a way to let experts learn the knowledge from others, it may improve the generalization of the models. To address that, based on the Mask Mechanism, we calculate the distance between the output of experts, to encourage each expert to guess the unseen part and make up the masked information. Due to the aim of MoE that choose different experts focusing knowledge, the Mean Squared Error (MSE) which measures the absolute error between two tensors, is not suitable for evaluating the similarity between the outputs of experts. Thus we choose the cosine distance to calculate the similarity between the output of each expert and not request the same. Specifically, we masked three experts, the remaining one could see all of the information and request three masked experts’ output similar to the remaining one. As shown in Algorithm 1, all of the outputs of the masked experts request to calculate the cosine distance with the unmasked one. Equation 3 denotes the calculation process.

$$\text{cosine_distance}_k = \frac{1}{s} \sum_{j=1}^s \sum_{i=2}^e \left(1 - \frac{\tilde{Y}_j^1 \tilde{Y}_j^i}{\|\tilde{Y}_j^1\| \|\tilde{Y}_j^i\|} \right) \quad (3)$$

\tilde{Y}_j^i denotes the j^{th} slot of the i^{th} Expert’s output. The Cosine Distance is the mean of the cosine similarity between the j^{th} slots of the two Experts. The e is the number of Experts and the s is the number of slots. The cosine_distance_k denotes the k^{th} residual block of ViT-B/16, which is the backbone of our image encoder. As shown in Equation 4, the cosine_distance is used to calculate our mmoe loss L_{mmoe} .

$$L_{\text{mmoe}} = \frac{1}{12} \sum_{k=1}^{12} \text{cosine_distance}_k \quad (4)$$

The ViT-B/16 consists of 12 residual blocks. Our mmoe loss, L_{mmoe} is mean of the 12 blocks’ Cosine Distance. This L_{mmoe} is added together with L_{clip} , which is the loss function of CLIP as shown in Equation 5.

$$L_{\text{clip}} = -\frac{1}{2N} \sum_{i=1}^N \left(\log \frac{\exp(S_{ii})}{\sum_{j=1}^N \exp(S_{ij})} + \log \frac{\exp(S_{ii})}{\sum_{j=1}^N \exp(S_{ji})} \right) \quad (5)$$

Algorithm 1: *Masked – MoE*

```

1: procedure MMOE( $X, e, s$ )
2:    $n, d \leftarrow X.\text{shape}$ 
3:    $\Phi \leftarrow \text{randn}(e, s, d)$ 
4:    $\text{logit} \leftarrow \text{einsum}(n, d, e, s, d \rightarrow n, e, s, X, \Phi)$ 
5:    $D \leftarrow \text{logits.softmax}(\text{dim} = 0)$ 
6:    $M \leftarrow \text{ones}([e, n, s])$ 
7:   for  $i$  in  $\text{range}(e)$  :
8:     if  $i \neq 0$  :
9:        $M[i][0 : n * s * 0.1] = 0$ 
10:    endif
11:     $\text{shuffle}(M[i])$ 
12:  endfor
13:   $D \leftarrow D * M$ 
14:   $C \leftarrow \text{rearrange}(\text{logits}, n, e, s \rightarrow n, (e, s))$ 
15:   $C \leftarrow C.\text{softmax}(\text{dim} = 1)$ 
16:   $\text{slots} \leftarrow \text{einsum}(n, d, n, e, s \rightarrow e, s, d, X, D)$ 
17:   $\text{out} \leftarrow \text{experts}(\text{slots})$ 
18:  for  $i$  in  $\text{range}(e)$  :
19:    if  $i \neq 0$  :
20:       $\text{mmoe\_loss} = \text{cosine}(\text{out}[0], \text{out}[i])$ 
21:    endif
22:  endfor
23:   $\text{out} \leftarrow \text{rearrange}(\text{out}, e, s, d \rightarrow (e, s), d)$ 
24:   $\text{out} \leftarrow \text{einsum}(s, d, n, s \rightarrow b, n, d, \text{out}, C)$ 
25:  return  $\text{out}$ 
26: end procedure

```

The loss function of CLIP model is a cross entropy between images and texts. The \mathbf{S} is the similarity matrix and the element S_{ij} of the similarity matrix \mathbf{S} denotes the similarity between the i^{th} image embedding and the j^{th} text embedding.

$$L_{\text{mmoe_with_clip}} = L_{\text{clip}} + L_{\text{mmoe}} \quad (6)$$

All of the loss function of our proposed MMoE with CLIP is shown as Equation 6.

Experiment

Datasets and Experimental Setting

We chose our proposed IrisGeneral as the dataset, the details are shown in the Section IrisGeneral Dataset with Table 1. All three protocols of the IrisGeneral listed in Table 2 are used. Protocol-1 evaluates the average performance of models in the iris anti-spoofing task, and Protocol-2 and Protocol-3 evaluate the cross-racial adaption and cross-device adaption respectively. We choose the Average Classification Error Rate (ACER), the Overall Detection Accuracy (ACC), the Area Under the Curve (AUC), and the Equivalent Error Rate (EER) as performance evaluation metrics. The experimental details are as follows: The backbone of CLIP’s image encoder is ViT-B/16. The mask rate is set as "0, 0.1, 0.1, 0.1.", and the prompts are set as "This is an image of <label>eye." We employ NVIDIA A100 GPUs to train and test with the Adam optimizer and the learning rate is 10^{-6} .

Method	Protocol-1				Protocol-2				Protocol-3 (Average)			
	ACER(%)↓	ACC(%)↑	AUC(%)↑	EER(%)↓	ACER(%)↓	ACC(%)↑	AUC(%)↑	EER(%)↓	ACER(%)↓	ACC(%)↑	AUC(%)↑	EER(%)↓
ResNet50	1.95	98.05	99.56	1.95	12.38	87.54	94.97	12.39	9.81	90.18	93.45	11.62
ViT-B/16	2.77	97.23	99.53	2.77	12.37	87.63	95.57	12.35	12.67	87.34	91.28	12.31
CLIP	1.41	98.59	99.61	1.41	8.09	91.91	97.82	8.11	6.85	93.14	95.53	8.97
FLIP	1.45	98.55	99.77	1.45	9.25	90.72	96.95	9.18	5.83	94.17	97.58	5.81
Ours	1.23	98.76	99.34	1.18	7.59	92.41	98.14	7.59	4.85	95.12	97.26	5.68

Table 3: This table shows the evaluation results on Protocol-1, Protocol-2, and Protocol-3 (Average).

Method	Protocol-3.1				Protocol-3.2				Protocol-3.3			
	ACER(%)↓	ACC(%)↑	AUC(%)↑	EER(%)↓	ACER(%)↓	ACC(%)↑	AUC(%)↑	EER(%)↓	ACER(%)↓	ACC(%)↑	AUC(%)↑	EER(%)↓
ResNet50	0.67	99.33	99.98	0.68	21.95	78.05	87.02	21.94	13.98	86.02	93.51	13.94
ViT-B/16	1.30	98.74	99.57	1.35	27.56	72.44	78.02	27.56	17.23	82.77	90.57	17.23
CLIP	1.34	98.66	99.94	1.35	19.60	80.39	88.46	19.64	6.21	93.79	97.97	6.19
FLIP	1.39	98.59	99.91	1.35	15.54	84.46	91.28	15.53	8.83	91.17	96.78	8.80
Ours	0.29	99.48	99.96	0.00	15.18	84.83	91.97	15.13	6.34	93.66	98.01	6.34

Method	Protocol-3.4				Protocol-3.5				Protocol-3.6			
	ACER(%)↓	ACC(%)↑	AUC(%)↑	EER(%)↓	ACER(%)↓	ACC(%)↑	AUC(%)↑	EER(%)↓	ACER(%)↓	ACC(%)↑	AUC(%)↑	EER(%)↓
ResNet50	20.87	79.13	80.26	31.98	0.97	98.97	99.93	0.77	0.43	99.57	99.99	0.40
ViT-B/16	26.71	73.29	79.94	24.62	1.03	98.97	99.92	0.92	2.19	97.81	99.68	2.20
CLIP	13.19	86.81	87.07	25.58	0.49	99.50	99.72	0.77	0.29	99.71	99.79	0.30
FLIP	8.30	91.70	97.73	8.28	0.52	99.47	99.76	0.62	0.38	99.62	99.99	0.30
Ours	6.57	93.43	93.90	11.94	0.50	99.50	99.69	0.46	0.19	99.81	100.00	0.20

Table 4: This table shows the specific evaluation results of each sub-protocol in Protocol-3.

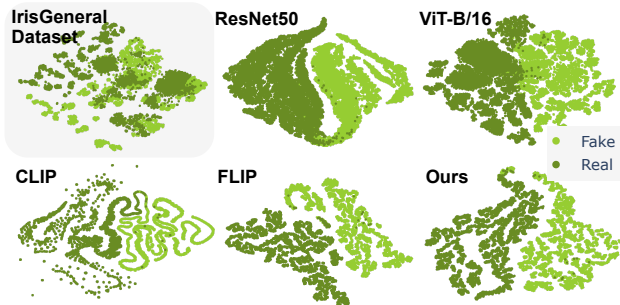


Figure 5: The feature distribution of each method on Protocol-1 of the IrisGeneral dataset. Our proposed method has the clearest border and regular shape.

Performance Evaluation

The ResNet50 (He et al. 2016), ViT-B/16 (Dosovitskiy et al. 2020), CLIP (Radford et al. 2021), and FLIP (Srivatsan, Naseer, and Nandakumar 2023) are chosen as representative models, then benchmarked them with ACER, ACC, AUC, and EER. Table 3 shows all the evaluation results including our proposed MMoE with CLIP and other models on Protocol-1, Protocol-2, and Protocol-3 (Average). Table 4 provides the specific results of each sub-protocol in Protocol-3. The evaluation results show that our proposed MMoE method with CLIP gets the best performance on both three protocols of the IrisGeneral dataset. For Protocol-

1, Ours achieves 1.23% ACER, which is a nearly 13% improvement compared to the vanilla CLIP with 1.41% ACER. It means that our MMoE method could effectively detect spoofing iris samples on all subsets of the IrisGeneral dataset and achieve SOTA performance. For Protocol-2, Ours achieves 7.59% ACER, much better than other previous models. It proves our proposed method has a high generalization ability on cross-racial challenges. Verified the effectiveness of our contributions. For Protocol-3, Ours achieves 4.85% ACER which has significant advantages over other previous models. It proves our proposed method also has a high generalization ability on cross-device challenges. In summary, above all the evaluations, our proposed MMoE method could effectively detect the spoofing iris images and perform high generalization on both cross-racial and cross-device situations. It achieves the SOTA performance on all protocols of the IrisGeneral dataset. Furthermore, Figure /reffig: distributions demonstrates the feature distribution of each method on Protocol-1. Our proposed method has the clearest border and regular shape in the latent space, showing its good ability in this iris anti-spoofing field.

Mask Rate Analysis

To discuss the impact of different rates of the mask, we set up 4 sets of mask rates and tested them on both Protocol-1 and Protocol-2. Among that, the first two sets mask the same rate for both three experts, and one expert could see

Mask-Rate Analysis Protocol-1				
Rates	ACER(%)↓	ACC(%)↑	AUC(%)↑	EER(%)↓
Rate_1	1.23	98.76	99.34	1.18
Rate_2	1.38	98.63	99.51	1.41
Rate_3	1.60	97.45	99.47	1.59
Rate_4	1.43	98.57	99.51	1.43
Mask-Rate Analysis Protocol-2				
Rates	ACER(%)↓	ACC(%)↑	AUC(%)↑	EER(%)↓
Rate_1	7.59	92.14	98.14	7.59
Rate_2	8.14	91.86	97.67	8.13
Rate_3	7.95	92.06	97.57	7.95
Rate_4	8.70	91.30	97.36	8.72

Table 5: The evaluation results of our MMoE with CLIP under different sets of mask-rates. The Rate_1 has the best performance on both Protocol-1 and Protocol-2.

all tokens with complete information. The third one masks different rates for three experts while one expert could also see all information as similar to the first two sets. The last one is quite different, in that all experts are masked part of tokens, which means the MMoE model could not gain the complete input. The details of each set are shown as follows:

Rate_1: 0, 0.1, 0.1, 0.1. **Rate_2:** 0, 0.5, 0.5, 0.5.

Rate_3: 0, 0.15, 0.3, 0.45. **Rate_4:** 0.1, 0.1, 0.1, 0.1.

According to the evaluation results shown in Table 5. The Rate_1 has the best performance on both Protocol-1 and Protocol-2, in which the ACERs are 1.23% and 7.59% respectively. The Rate_2 is a bit worse than the Rate_1 may caused by the high mask rate would make experts lose too much information and then influence the learning space of the MMoE model. The Rate_3 with different mask rates set has the worst performance on Protocol-1. This difference may increase the gap between the learning ability of experts and then cause a negative impact on the training process. The Rate_4 has a middle performance among these mask rate sets on Protocol-1, a bit worse than the Rate_1. And is the worst one on Protocol-2. This set makes the MMoE model could not gain the complete input information, which may influence the learning space.

Ablation Study

Two main contributions are proposed in our MMoE method: Mask Mechanism, and Cosine Distance Loss. To prove the effectiveness of our contributions, we provide the ablation study on Protocol-1 and Protocol-2. Among that, the **CLIP** means the vanilla CLIP framework, while **S** is SoftMoE, **L** is the cosine distance between experts, and **M** is the Mask Mechanism. So for example, **CLIP+S+M+L** means CLIP framework with SoftMoE, Mask Mechanism, and cosine distance between experts, it is briefly called MMoE with CLIP (Ours). The evaluation results are shown in Table 6, and the ACERs' trends are demonstrated in Figure 6. It could be observed that after adding the MoE "S" into the vanilla CLIP, the performance significantly declined, especially on Protocol-2, which may caused by the overfit-

Ablation Study Protocol-1				
Methods	ACER(%)↓	ACC(%)↑	AUC(%)↑	EER(%)↓
vanilla CLIP	1.41-	98.59-	99.61-	1.41-
CLIP+S	1.45↑	98.55↓	99.64↑	1.44↑
CLIP+S+L	1.31↓	98.70↑	99.34↓	1.40↓
CLIP+S+M	1.25↓	98.75↑	99.49↑	1.31↓
CLIP+S+M+L	1.23↓	98.76↑	99.34↓	1.18↓
Ablation Study Protocol-2				
Methods	ACER(%)↓	ACC(%)↑	AUC(%)↑	EER(%)↓
vanilla CLIP	8.09-	91.91-	97.82-	8.11-
CLIP+S	9.64↑	90.36↓	97.11↓	9.61↑
CLIP+S+L	7.60↓	92.40↑	98.03↑	7.60↓
CLIP+S+M	8.83↑	91.17↓	97.59↓	8.85↑
CLIP+S+M+L	7.59↓	92.41↑	98.14↑	7.59↓

Table 6: The evaluation results of each ablation on Protocol-1 and Protocol-2.

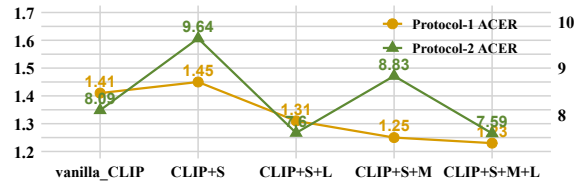


Figure 6: The ACER results of each ablation. It could be found that the addition of MoE "S" makes the model worse, which may be caused by overfitting. Our contributions L and M significantly alleviate this problem and effectively improve the generalization performance.

ting problem of introducing MoE. After adding our contributions L and M, the performances improved on both Protocols. Specifically, to compare the ablation results, the CLIP+S+L is better on Protocol-2 which focuses on generalization, while the CLIP+S+M is better on Protocol-1 which focuses on average performance. That proves our contributions Cosine Distance Loss "L" could improve the model's generalization ability and Mask Mechanism "M" significantly alleviates the overfitting caused by MoE. The CLIP+S+M+L (Ours) shows the best performance among these combined models, the ACER is 1.23% on Protocol-1 and 7.59% on Protocol-2. That good performance is thanks to both alleviating overfitting and improving generalization with our two contributions.

Conclusion and Future Work

In this paper, we proposed a unified framework for iris anti-spoofing, which includes an IrisGeneral dataset and the Mased-MoE method. It significantly improves the generalization of iris anti-spoofing models and alleviates overfitting problems. In future work, we will focus on studying the boundary of the MMoE's adaptive capability.

References

- Aceña, V.; de Diego, I. M.; Fernández, R. R.; and Moguerza, J. M. 2022. Minimally overfitted learners: a general framework for ensemble learning. *Knowledge-Based Systems*, 254: 109669.
- Agarwal, R.; and Jalal, A. S. 2021. Presentation attack detection system for fake Iris: a review. *Multimedia Tools and Applications*, 80: 15193–15214.
- Allingham, J. U.; Wenzel, F.; Mariet, Z. E.; Mustafa, B.; Puigcerver, J.; Houlsby, N.; Jerfel, G.; Fortuin, V.; Lakshminarayanan, B.; Snoek, J.; et al. 2021. Sparse MoEs meet efficient ensembles. *arXiv preprint arXiv:2110.03360*.
- Bowyer, K. W.; and Doyle, J. S. 2014. Cosmetic contact lenses and iris recognition spoofing. *Computer*, 47(5): 96–98.
- Boyd, A.; Tinsley, P.; Bowyer, K.; and Czajka, A. 2021. Cyborg: Blending human saliency into the loss improves deep learning. *arXiv preprint arXiv:2112.00686*.
- Cai, W.; Jiang, J.; Wang, F.; Tang, J.; Kim, S.; and Huang, J. 2024. A survey on mixture of experts. *arXiv preprint arXiv:2407.06204*.
- Chang, C.-Y.; Hsu, M.-T.; Esposito, E. X.; and Tseng, Y. J. 2013. Oversampling to overcome overfitting: exploring the relationship between data set composition, molecular descriptors, and predictive modeling methods. *Journal of chemical information and modeling*, 53(4): 958–971.
- Chen, T.; Zhang, Z.; Jaiswal, A.; Liu, S.; and Wang, Z. 2023. Sparse moe as the new dropout: Scaling dense and self-slimmable transformers. *arXiv preprint arXiv:2303.01610*.
- Daugman, J. 2009. How iris recognition works. In *The essential guide to image processing*, 715–739. Elsevier.
- Dosovitskiy, A.; Beyer, L.; Kolesnikov, A.; Weissenborn, D.; Zhai, X.; Unterthiner, T.; Dehghani, M.; Minderer, M.; Heigold, G.; Gelly, S.; et al. 2020. An image is worth 16x16 words: Transformers for image recognition at scale. *arXiv preprint arXiv:2010.11929*.
- Doyle, J.; and Bowyer, K. 2014. Notre Dame Image Database for Contact Lens Detection in Iris Recognition—2013. *Data Sets*. [html](#).
- Elbayad, M.; Sun, A.; and Bhosale, S. 2022. Fixing MoE over-fitting on low-resource languages in multilingual machine translation. *arXiv preprint arXiv:2212.07571*.
- Galbally, J.; Ortiz-Lopez, J.; Fierrez, J.; and Ortega-Garcia, J. 2012. Iris liveness detection based on quality related features. In *2012 5th IAPR International Conference on Biometrics (ICB)*, 271–276. IEEE.
- Gent, E. 2023. A Cryptocurrency for the Masses or a Universal ID?: Worldcoin Aims to Scan all the World’s Eyeballs. *IEEE Spectrum*, 60(1): 42–57.
- Goodfellow, I.; Pouget-Abadie, J.; Mirza, M.; Xu, B.; Warde-Farley, D.; Ozair, S.; Courville, A.; and Bengio, Y. 2014. Generative adversarial nets. *Advances in neural information processing systems*, 27.
- He, K.; Chen, X.; Xie, S.; Li, Y.; Dollár, P.; and Girshick, R. 2022. Masked autoencoders are scalable vision learners. In *Proceedings of the IEEE/CVF conference on computer vision and pattern recognition*, 16000–16009.
- He, K.; Zhang, X.; Ren, S.; and Sun, J. 2016. Deep residual learning for image recognition. In *Proceedings of the IEEE conference on computer vision and pattern recognition*, 770–778.
- He, X.; An, S.; and Shi, P. 2007. Statistical texture analysis-based approach for fake iris detection using support vector machines. In *Advances in Biometrics: International Conference, ICB 2007, Seoul, Korea, August 27-29, 2007. Proceedings*, 540–546. Springer.
- Jacobs, R. A.; Jordan, M. I.; Nowlan, S. J.; and Hinton, G. E. 1991. Adaptive mixtures of local experts. *Neural computation*, 3(1): 79–87.
- Kingma, D. P.; and Welling, M. 2013. Auto-encoding variational bayes. *arXiv preprint arXiv:1312.6114*.
- Komulainen, J.; Hadid, A.; and Pietikäinen, M. 2014. Generalized textured contact lens detection by extracting bsif description from cartesian iris images. In *IEEE International Joint Conference on Biometrics*, 1–7. IEEE.
- Kumar, S.; Lamba, V. K.; and Jangra, S. 2020. Anti-Spoofing for Iris Recognition With Contact Lens Detection. *Adv Appl Math Sci*, 19(5): 397–406.
- LeCun, Y.; Bottou, L.; Bengio, Y.; and Haffner, P. 1998. Gradient-based learning applied to document recognition. *Proceedings of the IEEE*, 86(11): 2278–2324.
- Lepikhin, D.; Lee, H.; Xu, Y.; Chen, D.; Firat, O.; Huang, Y.; Krikun, M.; Shazeer, N.; and Chen, Z. 2020. Gshard: Scaling giant models with conditional computation and automatic sharding. *arXiv preprint arXiv:2006.16668*.
- Long, M.; Cao, Y.; Wang, J.; and Jordan, M. 2015. Learning transferable features with deep adaptation networks. In *International conference on machine learning*, 97–105. PMLR.
- Long, M.; Zhu, H.; Wang, J.; and Jordan, M. I. 2017. Deep transfer learning with joint adaptation networks. In *International conference on machine learning*, 2208–2217. PMLR.
- Nigam, I.; Vatsa, M.; and Singh, R. 2015. Ocular biometrics: A survey of modalities and fusion approaches. *Information Fusion*, 26: 1–35.
- Perala, A. 2017. Princeton identity tech powers galaxy s8 iris scanning.
- Puigcerver, J.; Riquelme, C.; Mustafa, B.; and Houlsby, N. 2023. From sparse to soft mixtures of experts. *arXiv preprint arXiv:2308.00951*.
- Radford, A.; Kim, J. W.; Hallacy, C.; Ramesh, A.; Goh, G.; Agarwal, S.; Sastry, G.; Askell, A.; Mishkin, P.; Clark, J.; et al. 2021. Learning transferable visual models from natural language supervision. In *International conference on machine learning*, 8748–8763. PMLR.
- Ren, C.-X.; Ge, P.; Yang, P.; and Yan, S. 2020. Learning target-domain-specific classifier for partial domain adaptation. *IEEE Transactions on neural networks and learning systems*, 32(5): 1989–2001.

- Shazeer, N.; Mirhoseini, A.; Maziarz, K.; Davis, A.; Le, Q.; Hinton, G.; and Dean, J. 2017. Outrageously large neural networks: The sparsely-gated mixture-of-experts layer. *arXiv preprint arXiv:1701.06538*.
- Srivatsan, K.; Naseer, M.; and Nandakumar, K. 2023. Flip: Cross-domain face anti-spoofing with language guidance. In *Proceedings of the IEEE/CVF International Conference on Computer Vision*, 19685–19696.
- Sun, Z.; Zhang, H.; Tan, T.; and Wang, J. 2014. Iris Image Classification Based on Hierarchical Visual Codebook. *IEEE Transactions on Pattern Analysis and Machine Intelligence*, 36(6): 1120–1133.
- Tinsley, P.; Flynn, P.; and Czajka, A. 2024. *Trust, AI, and Synthetic Biometrics*. Ph.D. thesis, University of Notre Dame.
- Tzeng, E.; Hoffman, J.; Saenko, K.; and Darrell, T. 2017. Adversarial discriminative domain adaptation. In *Proceedings of the IEEE conference on computer vision and pattern recognition*, 7167–7176.
- Wei, Z.; Qiu, X.; Sun, Z.; and Tan, T. 2008. Counterfeit iris detection based on texture analysis. In *2008 19th International Conference on Pattern Recognition*, 1–4. IEEE.
- Xiao, L.; Sun, Z.; He, R.; and Tan, T. 2013. Coupled feature selection for cross-sensor iris recognition. In *2013 IEEE Sixth International Conference on Biometrics: Theory, Applications and Systems (BTAS)*, 1–6. IEEE.
- Xie, Y.; Huang, S.; Chen, T.; and Wei, F. 2023. Moec: Mixture of expert clusters. In *Proceedings of the AAAI Conference on Artificial Intelligence*, volume 37, 13807–13815.
- Yadav, D.; Kohli, N.; Doyle, J. S.; Singh, R.; Vatsa, M.; and Bowyer, K. W. 2014a. Unraveling the effect of textured contact lenses on iris recognition. *IEEE Transactions on Information Forensics and Security*, 9(5): 851–862.
- Yadav, D.; Kohli, N.; Doyle, J. S.; Singh, R.; Vatsa, M.; and Bowyer, K. W. 2014b. Unraveling the effect of textured contact lenses on iris recognition. *IEEE Transactions on Information Forensics and Security*, 9(5): 851–862.
- Yadav, S.; Chen, C.; and Ross, A. 2019. Synthesizing iris images using RaSGAN with application in presentation attack detection. In *Proceedings of the IEEE/CVF conference on computer vision and pattern recognition workshops*, 0–0.
- Yadav, S.; Chen, C.; and Ross, A. 2020. Relativistic discriminator: A one-class classifier for generalized iris presentation attack detection. In *Proceedings of the IEEE/CVF Winter Conference on Applications of Computer Vision*, 2635–2644.
- Yadav, S.; and Ross, A. 2024. Synthesizing Iris Images using Generative Adversarial Networks: Survey and Comparative Analysis. *arXiv preprint arXiv:2404.17105*.
- Yambay, D.; Becker, B.; Kohli, N.; Yadav, D.; Czajka, A.; Bowyer, K. W.; Schuckers, S.; Singh, R.; Vatsa, M.; Noore, A.; et al. 2017. LivDet iris 2017—Iris liveness detection competition 2017. In *2017 IEEE International Joint Conference on Biometrics (IJCB)*, 733–741. IEEE.
- Zhang, H.; Bai, Y.; Zhang, H.; Liu, J.; Li, X.; and He, Z. 2021. Local attention and global representation collaborating for fine-grained classification. In *2020 25th International Conference on Pattern Recognition (ICPR)*, 10658–10665. IEEE.
- Zou, H.; Zhang, H.; Li, X.; Liu, J.; and He, Z. 2018. Generation textured contact lenses iris images based on 4dcycle-gan. In *2018 24th International Conference on Pattern Recognition (ICPR)*, 3561–3566. IEEE.